HHS Public Access

Author manuscript

IEEE Biomed Circuits Syst Conf. Author manuscript; available in PMC 2020 February 14.

Published in final edited form as:

IEEE Biomed Circuits Syst Conf. 2018 October ; 2018: . doi:10.1109/BIOCAS.2018.8584729.

Low-cost, Implantable Wireless Sensor Platform for Neuromodulation Research

Ian McAdams[1,2], **Hannah Kenyon**[1], **Dennis Bourbeau**[3], **Margot S. Damaser**[1,4,5], **Christian Zorman**[1,2,4], **Steve J.A. Majerus**[1,5]

[1]Dept. of Biomedical Engineering, Lerner Research Institute

[2]Dept. of Electrical Engineering and Computer Science Case Western Reserve University Cleveland, Ohio, USA

[3]Functional Electrical Stimulation Center

[4]Glickman Urological and Kidney Institute Cleveland Clinic

[5]Advanced Platform Technology Center Louis Stokes Veterans Affairs Medical Center Cleveland, Ohio, USA

Abstract

The role of peripheral nerves in regulating major organ function in health and disease is not well understood. Elucidating the relationships between biomarkers and neural activity during conditions free form anesthesia is essential to advancing future investigations of autonomic organ control and improving precision for neuromodulation treatment approaches. Here we present a simple, customizable, off-the-shelf component sensor platform to meet research needs for studying different organs under conscious, free movement. The platform consists of a small, rechargeable coin-cell battery, an energy-harvesting IC, a low-power microcontroller, a low-power pressure transducer, customizable number of electrodes with a common anode, inductive recharge input, and OOK inductive transmission. A case study demonstrating a bladder implant for long-term monitoring is presented, utilizing a novel, non-hermetic encapsulation approach. The customized platform uses two sleep modes to minimize battery loading, exhibiting a maximum time-averaged current draw of 125 micro-amps during sensing and transmission, with a quiescent current draw of 95 nano-amps into the microcontroller.

I. Introduction

Although the organs of the human body differ greatly in function and cellular physiology, they are all stimulated and controlled in some fashion, by the nervous system. Previous efforts to map the brain and central nervous system spawned multiple therapies to treat neurodegenerative disorders [1,2], however, little research has focused on the peripheral nervous system and its interplay with organ function [3]. Coordinated efforts to understand the role of the peripheral nerves in organ control are underway, such as the Stimulating Peripheral Activity to Relieve Conditions (SPARC) program of the National Institutes of Health (NIH). This ongoing effort to map and understand peripheral nerve-organ interactions seeks to advance the precision with which organs can be treated through electrical nerve stimulation (neuromodulation). Improved neuromodulation could provide

treatment for a range of medical conditions such as hypertension, diabetes, and inflammatory conditions, or could target organ-specific disorders such as heart failure, neurogenic bladder and bowel dysfunction, or gastric motility disorders.

Unlike neural recording and mapping in the central nervous system, detection of the nerve-organ interaction requires measures of nervous activity paired with functional measures of organ activity. Therefore, customized sensors are needed to meet the anatomical size limits of organs being monitored, to interface with the organ bio-environment without causing toxicity, and to provide appropriate transduction of organ function. Furthermore, neuromodulation treatment studies will require tools for conscious monitoring of organ function, because long-term outcomes cannot be detected under anesthesia. Therefore, organ-specific sensors which can be implanted for preclinical research studies, are required to accelerate neuromodulation research.

Here, we present a simple sensor platform which can be customized in form and function to meet the research needs for different organs in conscious, freely-moving animals. Because the sensor is based on commercial, off-the-shelf components, customizable software, and a nonhermetic encapsulation procedure, it can be adopted and modified for various research applications. This sensor was developed as a scientific tool for the neuromodulation community, and specific details on the circuitry and software are available upon request so the device may be customized and used for particular applications.

Although we have developed three variants of this sensor, here we will focus only on the sensor electronic architecture and present a bladder pressure- and volume-sensing device as an example case study of the utility of the sensor platform.

II. Sensor Platform Architecture

A. Sensor Data Acquisition

The wireless sensor platform was built around the functionality and peripheral circuitry included in common, commercial microcontrollers (Fig. 1a). These devices are now small enough to consider for miniaturized biomedical implants, and the combination of reconfigurable functionality and customizable software is clearly superior for research tools. For the bladder sensor discussed later, a MSP430-series device (MSP430FR2532, Texas Instruments) forms the core of the sensor architecture.

In a representative configuration (Fig. 1a), 4 sensors are included which interface with the bio-media. Sensors can measure conductance or impedance of media using inert electrode materials like platinum or graphite. Peripheral analog circuitry such as an ADC or capacitive touch interface module are common and can be used for analog measurement. Other integrated sensors—such as pressure sensors—communicate with the microcontroller using common serial schemes. This architecture can potentially include many types of sensors and sensing methods, including impedance spectroscopy or cyclic voltammetry using customized electrode coatings to detect biomarkers.

B. Wireless Data Transmission

Data transmission from a wireless implantable device is usually the most power-intensive system function. Tradeoffs involving antenna efficiency, frequency-dependent tissue absorption, device size, and RF transmitter overhead must be considered, especially when the system battery has limited output capacity. For deeply-implanted devices, low RF frequencies have significantly less tissue absorption and can be transmitted with simple circuitry. Due to the long wavelength, however, low RF antennas are operated in near-field modes in which signal transmission is effectively inductive. This permits the use of sub-wavelength magnetic antennas, which are small and require no RF reflector planes. For the sensor platform, an inductive winding can be directly driven from the microcontroller in a single-ended or push-pull configuration. On-off-keying (OOK) modulation is used to conserve power, and data is transmitted in RF bursts as digital packets.

This transmission scheme is simple to implement, but inefficient at distances greater than 10-20 cm. However, in many research settings this range is appropriate, and data is captured by a low-RF radio receiver worn on the animal or used during experiments. Onboard storage, e.g. to an SD card, or standard RF transmission, e.g. Bluetooth, is used from the receiver to a remote monitoring system so that data can be logged from the animal without tethering.

C. Wireless Battery Charging

To maintain a small implant size, a miniature rechargeable 5.5 mAh lithium battery is used (Seiko MS621 FE). An RF-DC energy harvester (ST-Micro SPV1050) is coupled to an inductive antenna tuned to 6.78 MHz for wireless energy capture. The antenna is coupled to a Schottky diode-based RF voltage doubler circuit, providing low-level DC input to the energy harvester. A switch-mode circuit boosts the small input current to a voltage large enough to recharge the 3.0-V battery. Recharge time can be adjusted based on depth of implant, sensor size, and antenna area. In typical 10-20 cm implant depth applications, recharge currents of 100 μA can be achieved [4,5].

D. Software Architecture, Sleep Modes, & GPIO Wake-up

The application software is written as a circular state machine, in which real-time task scheduling is not needed (Fig. 1b). Instead, the microcontroller spends most of its time in a “nap” state, where only a real-time clock is running. At regular timer intervals, an interrupt wakes the CPU and sensor data acquisition is performed. After a programmable period of data transmission, the device enters a “deep sleep” state in which everything is powered down. The device remains in deep sleep until it receives a high-to-low signal edge from the RF-DC energy harvester, which occurs when the external battery recharge field is applied.

III. Example Bladder Sensor for Research

There is a need in both research and clinical applications for long-term, catheter-free, ambulatory bladder state monitoring. Bladder volume and pressure are biomechanical variables that cause changes in peripheral nerve activity, and which can be modulated by stimulating the nerves of the pelvic floor. One use case for this sensor platform is conscious

monitoring of the feline bladder. This animal was chosen because it is an established model for pelvic neural research, because it maintains physiologic bladder function under long periods of anesthesia, facilitating neural recording.

Because the feline bladder is small (30 – 50 mL typically in males), and the urethra is narrow (less than 1 mm diameter), it cannot be accessed using a cystoscope or similar instrument for implantation. Therefore, bladder sensors must be surgically implanted within the bladder. Prior attempts using wired sensors crossing the bladder wall caused tissue erosion and damage [6,7], so we developed a sensor to be placed directly in the hollow bladder lumen. This device form factor and sensing modes were based on the platform described above, and a simple nonhermetic polymer encapsulation was used to provide biocompatible moisture protection and resistance to urine corrosion. The assembled sensor measured 12 x 18 mm, with a thickness of 3.7 mm and an approximate volume of 0.7 cm^3 (Fig. 2). Here each feature is described in detail.

A. Volume- and Pressure-Sensing Modes

The volume sensing module consists of two cathodes and a common anode (Fig. 1a, Fig. 2) which are exposed to urine in the bladder. During sensing, a small current is passed between the electrodes, occurring via ionic polarization, where the total cathodic current is proportional to the total number of ions. Therefore, the sensor current is determined both by the volume of urine (number of ions) and the concentration of urine (density of ions). To correct for changes in urine concentration throughout the day, electrodes are arranged so that two currents are passed through different equivalent urine volumes. A short path current (I_{C1}) flows through a roughly constant, small volume and is dependent solely on urine concentration. The longer current path (I_{C2}) flows through the larger volume of urine in the bladder and is proportional to both urine volume and concentration. A corrected sensor current, I_S, is computed simply as the ratio between I_{ci} and I_{C2}.

The volume-sensing module is designed to detect natural bladder filling cycles, which take up to hours even in small research animals. Because the conduction-mode sensor requires significant energy per sample, urine volume is only measured once per 5 seconds (0.2 Hz sample rate), which is still sufficient after averaging to produce at least one mean value of urine volume per minute. Bladder pressure, on the other hand, varies quite rapidly, especially when the bladder muscle actively contracts or in the presence of motion. To prevent aliasing, pressure is oversampled at 10 Hz, then filtered in software using an exponential moving average filter to a 1 Hz equivalent bandwidth, which is sufficient to detect contractions but rejects many abdominal pressure artifacts [9].

B. Non-Hermetic Device Encapsulation

In a research setting, hermetic feedthrough technologies add significant cost and limit the ability to change device form factors or functionality. Therefore, the feline bladder sensor was encapsulated simply using readily-available non-hermetic encapsulants. After components are soldered, platinum mesh electrodes were brazed to the circuit board. A medical epoxy (Loctite EA M-31 CL) was applied around the board perimeter (excluding the mesh electrodes), and epoxy was used to fill in between all the electronic components.

After this basic encapsulation, the epoxy was sufficient for waterproofing. However, because the inner bladder lining is easily irritated, an outer layer of polydimethylsiloxane (PDMS) (Dow Corning Sylgard 184) was added to the device exterior to provide a soft coating and cover the pressure sensor so that urine pressure can be transduced. The pressure sensor encapsulation employs a previously-used procedure [8] in which the silicon membrane transduction surface is covered in an incompressible silicone gel and overlaid with a thin, nylon mesh-reinforced layer of PDMS (Fig. 3).

IV. In Vitro and In Vivo Sensor Testing

A. Sensor Calibration, Performance, & Power Consumption

Wired sensor prototypes were encapsulated as described above and tested *in vitro*. Pressure sensors were calibrated in a 0.9% saline-filled pressure chamber against standard in-line blood pressure reference sensors. Pressure sensing performance was fairly linear over a physiologic pressure range of 0 – 200 cmH_2O, with an RMS error of 1.9 cmH2O representing 1.08% error full-scale. Sensors did show a slow drift over time (Fig. 4) which could have been due to moisture uptake in the PDMS gel. This drift was slower than typical bladder contractions and could therefore be rejected, although this might affect static pressure measurement accuracy.

Wired sensor volume- and concentration-sensing performance was validated *in vitro* in 50-mL latex balloons suspended in a saline bath. Balloons were filled with either known concentrations of saline, or samples of feline urine collected from research studies; this environment simulated the geometry and contents of the actual feline bladder. A precision syringe pump was used to infuse and extract the urine samples at a fixed volumetric rate. Concentration sensor performance was validated using solutions of 0.1 – 4.0 % aqueous sodium chloride (saline) to represent the range of feline urine concentrations (Fig. 4). Actual solution conductivities were validated using clinical conductivity meter (Mettler-Toledo FiveGo F3). The sensor demonstrated a monotonic response curve with sufficient accuracy to detect between several ranges of concentration.

Next, the concentration-corrected volume sensor performance was tested using 4 samples of feline urine obtained from animal studies. Each sample was exposed to the sensor, and equivalent volumes were calculated as the ratio of I_{C1} and I_{C2} currents as described previously. The volume sensor error across all trials revealed a volume-dependent error which increased greatly above 25 mL (Fig. 5). In the typical feline bladder capacity range of 0 – 40 mL, however, the volume sensor demonstrated a concentration-independent average volume sensing accuracy better than 5mL. The sensor accuracy, while low, still provides a sufficient measure of bladder fullness to enable neuromodulation research.

The sensor power consumption varies greatly throughout the data acquisition and transmission cycle. Total power draw from the battery was measured by Texas Instrument EnergyTrace software (Fig. 6) and a wired sensor. The sensor was exposed to 4% concentrated saline to measure the worst-case current draw while measuring urine volume. The table in Fig. 6 summarizes the bladder sensor power consumption per mode. Deep sleep

mode exhibits 1.5 μA, though this was dominated by the pressure sensor standby current, and the microcontroller current draw in deep sleep was 95 nA.

B. 30-day Device Implantation in Feline Bladder

A non-functional sensor module with the same components and form factor as Fig. 2 was encapsulated and sterilized for implantation to study surgical implantation, animal recovery, and device tolerability over a 30-day period. The animal did not demonstrate any behavioral or urinary frequency changes, suggesting good tolerance of the device in the bladder. Urinalysis obtained throughout this period showed no urinary tract infections, but a slight increase in urine nickel content which might have been due to the device. Overall this initial experiment suggested that the sensor geometry and surgical implantation is feasible even for research animals as small as felines (Fig. 7).

V. Conclusion

The low-power, implant sensor platform was designed, prototyped, and tested through a case study of the feline bladder. Preliminary feedback from a non-functional sham implant of the correct form factor and encapsulation suggests good tolerability by the animal. The bladder implant platform utilized two sleep modes to minimize average power draw, measuring conductance at 0.2Hz and pressure at 10Hz when active, while also transmitting data at 10Hz. Under worst-case load conditions, the active power draw into the microcontroller is 125 μA, yielding an estimated ~40 hours of active mode lifetime prior to recharge, with the selected battery. A low-power, customizable sensor platform such as this would improve studies of peripheral nerve-organ interaction and improve the precision of neuromodulation treatments.

Acknowledgments

This work was funded by the NIH Stimulating Peripheral Activity to Relieve Conditions (SPARC) program, NIH grant number OT2OD023873.

References

[1]. Hall PA, Bickel WK, Erickson KI and Wagner DD, “Neuroimaging, neuromodulation, and population health: the neuroscience of chronic disease prevention.” Ann N Y Acad Sci, Epub ahead of print, 2018.

[2]. Koroshetz W et al. “The State of the NIH BRAIN Initiative.” Jour Neuroscience, Epub ahead of print, 2018.

[3]. Goroszeniuk T and Pang D, “Peripheral neuromodulation: a review.” Curr Pain Headache Rep, vol. 18, no. 5, 2014.

[4]. Yakovlev A, Kim S and Poon A, "Implantable biomedical devices: Wireless powering and communication," in IEEE Communications Magazine, vol. 50, no. 4, pp. 152–159, 4 2012.

[5]. Liu C, Jiang C, Song J and Chau KT, "An Effective Sandwiched Wireless Power Transfer System for Charging Implantable Cardiac Pacemaker," in IEEE Transactions on Industrial Electronics, Epub ahead of print.

[6]. Melgaard J & Rijkhoff NJM Detecting the onset of urinary bladder contractions using an implantable pressure sensor. IEEE Trans Neural Syst Rehabil Eng 19 700–708 (2011). [PubMed: 21997323]

[7]. Basu A, Majerus S, Ferry L, Makovey I, Zhu H, Damaser MS, “Is submucosal bladder pressure monitoring feasible?” Journal of Engineering in Medicine – in press 9 2017.

[8]. Majerus S, Fletter PC, Ferry EK, Zhu H, Gustafson KJ, Damaser MS (2016) “Suburothelial Bladder Contraction Detection with Implanted Pressure Sensor.”PLoS One. 2017 1 6;12(1):e0168375 [PubMed: 28060842]

[9]. Karam R, Bourbeau D, Majerus S, Makovey I, Goldman HB, Damaser MS, Bhunia S, "Real-Time Classification of Bladder Events for Effective Diagnosis and Treatment of Urinary Incontinence," IEEE Transactions on Biomedical Engineering, vol. 63, no. 4, 4 2016, pp. 721–729. [PubMed: 26292331]

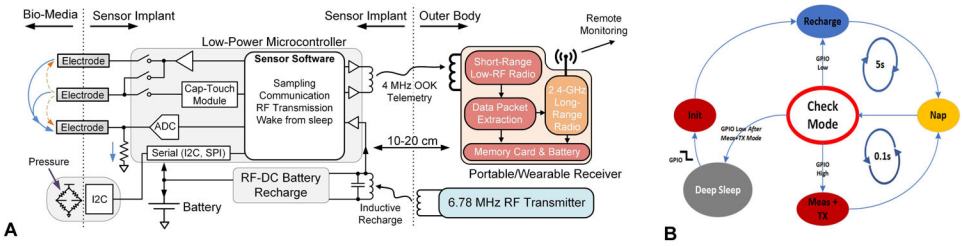

Fig. 1.

The sensor platform architecture is shown for a bladder monitoring study (a). A low-power microcontroller and RF energy harvester are the core ICs for the implanted device. Reconfigurable I/O of the microcontroller enables a variety of bio-media sensors, such as conductance- and capacitive-sensing electrodes and an integrated pressure sensor. An external receiver picks up data packets from the implant transmitted using on-off-keying (OOK) and a 6.78-MHz inductive charger is used for battery recharge of the implant. The application software runs a simple state machine (B) based on the sensing requirements for the target organ. Power-managed modes are used extensively to reduce overall power consumption.

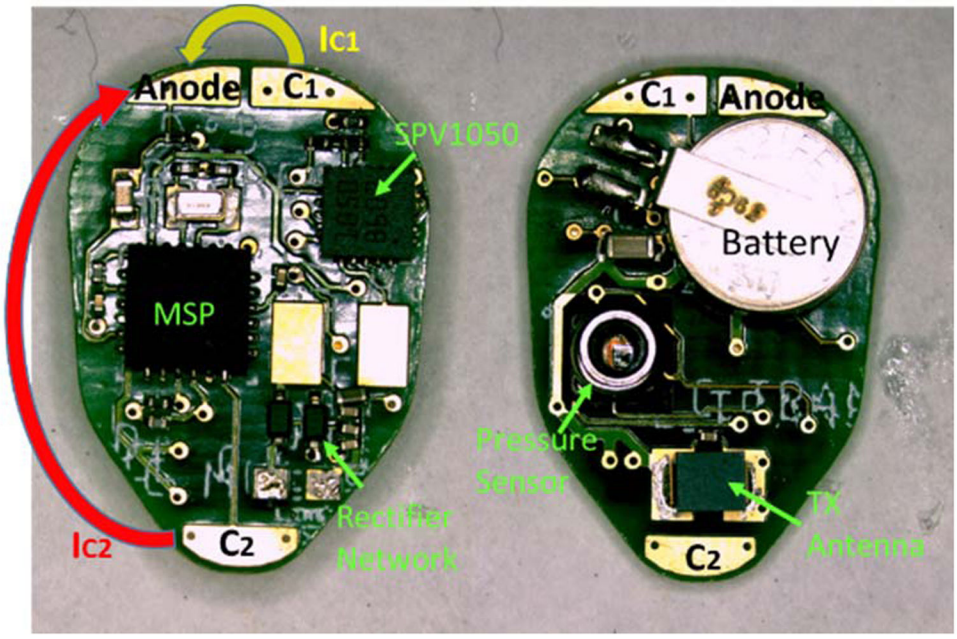

Fig. 2:

The fabricated sensor for bladder monitoring included a pressure sensor and solder pads for urine volume measurement. Platinum electrodes (not shown) are soldered to the pads prior to device encapsulation.

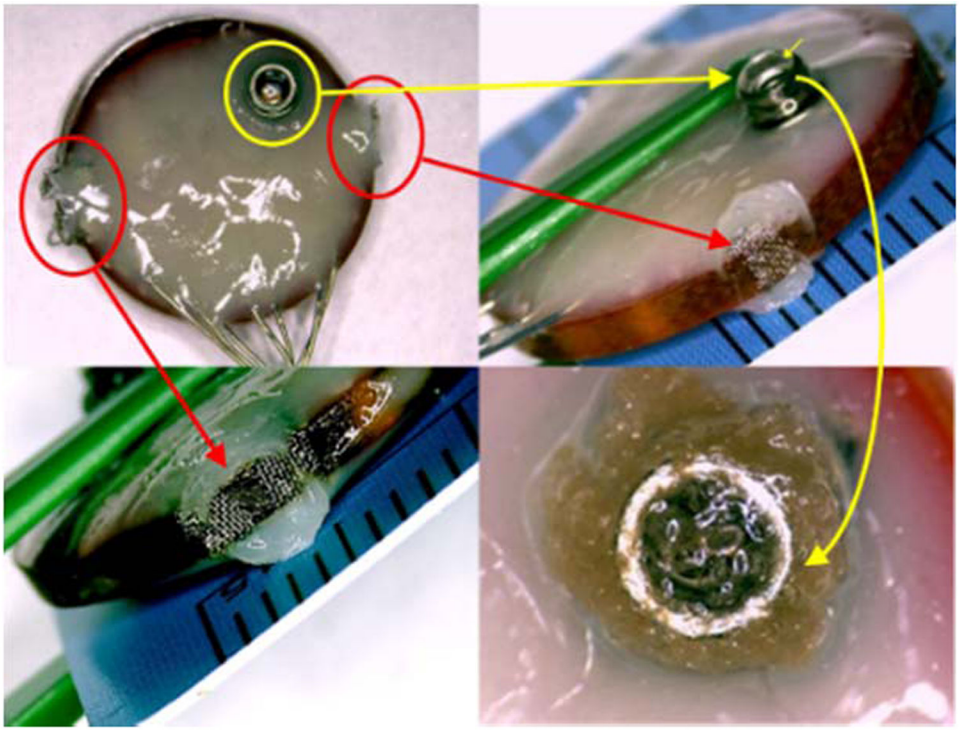

Fig. 3:
Image of an encapsulated, wired sensor prototype with cathodes and anode (red), and pressure sensor with nylon-reinforced PDMS layer (yellow).

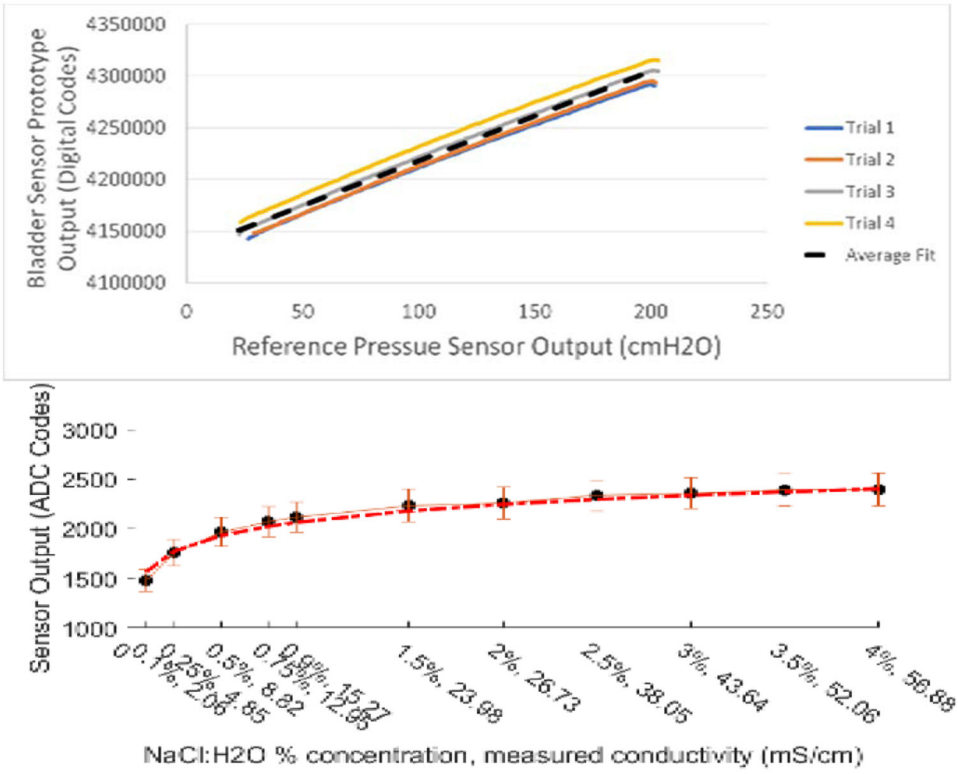

Fig. 4.

(Top) Reference pressure sensor output vs. platform sensor output over four repeat trials, with average transfer function overlaid (black). (Bottom) Mean C_1 cathode output vs. saline conductivity from a commercial probe. Data points are the mean and standard deviation of four prototypes.

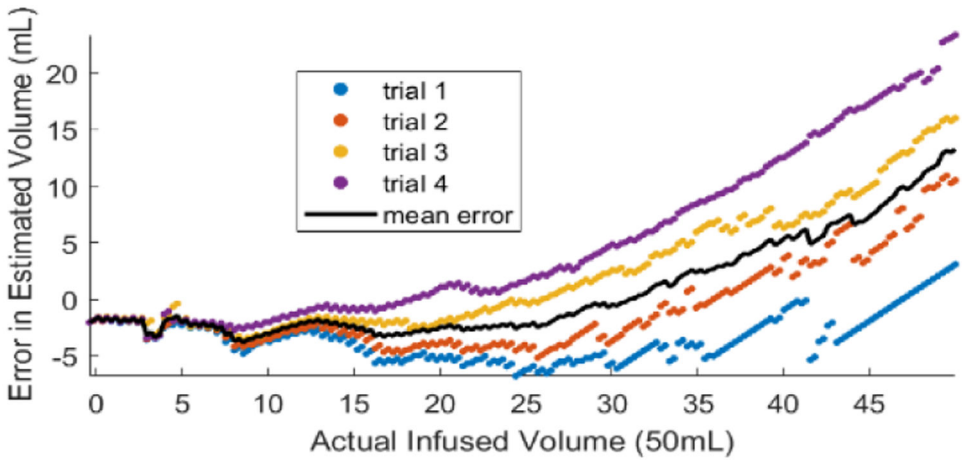

Fig. 5.

Linearized sensor output error of volume predictions in cat urine, with mean error (black line) and repeat trials in color.

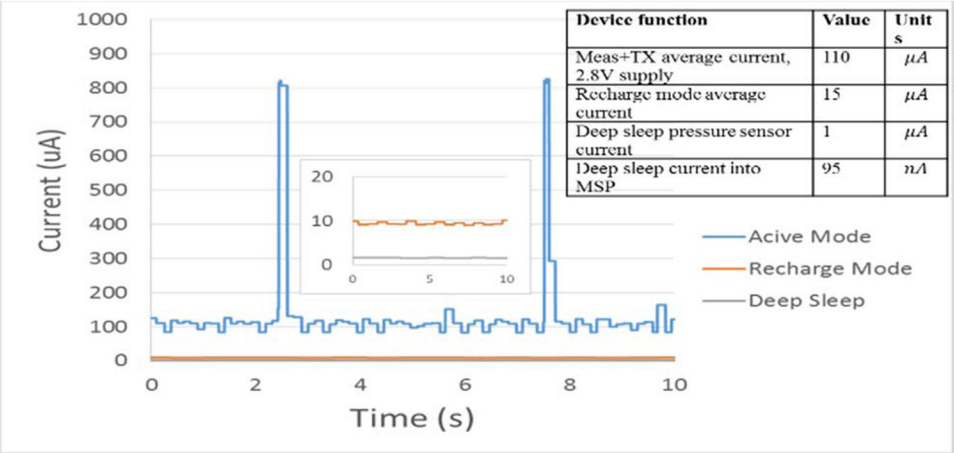

Device function	Value	Unit s
Meas+TX average current, 2.8V supply	110	μA
Recharge mode average current	15	μA
Deep sleep pressure sensor current	1	μA
Deep sleep current into MSP	95	nA

Fig. 6.

Measured sensor power draw in active measurement (125 μA), recharge (15 μA), and deep sleep (1.5 μA) modes. Sensor current draw varies dynamically, with the largest power draw occurring during volume measurement phases. This accommodates ~40 hours of active mode function prior to recharge.

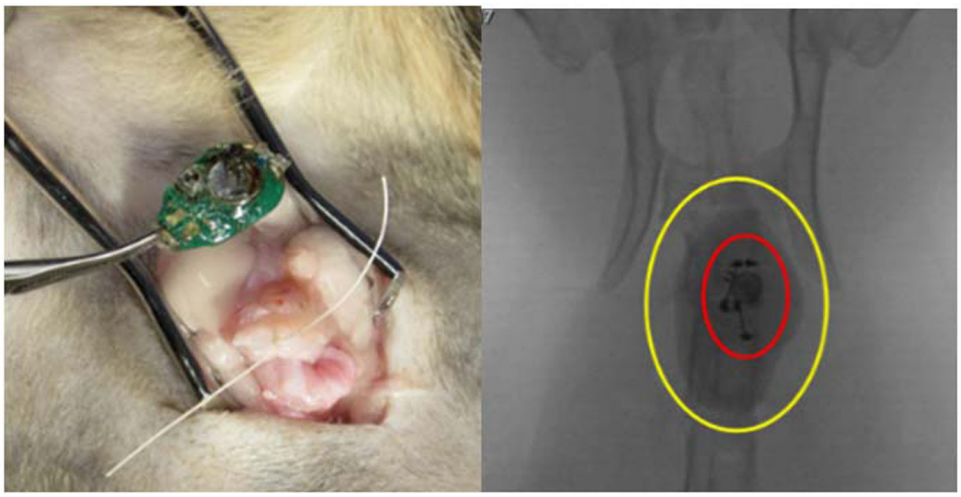

Fig. 7.

(Left) exposed bladder with sham device. (Right) Fluoroscopy image of implanted, non-functional sham device (red) in feline bladder (yellow). The animal showed no signs of discomfort or change in urinary behavior over the 30-day implant period.